ELSEVIER

Journal of Power Sources 111 (2002) 65–82

JOURNAL OF POWER SOURCES

www.elsevier.com/locate/jpowsour

Evaluation of VRLA battery under overcharging: model for battery testing

A. Tenno[a,*], R. Tenno[a], T. Suntio[b]

[a]*Control Engineering Laboratory, Helsinki University of Technology, P.O. Box 5400, FIN-02015 Espoo, Finland*
[b]*Electronics Laboratory, University of Oulu, P.O. Box 4500, FIN-90014 Oulu, Finland*

Received 30 June 2001; received in revised form 16 April 2002; accepted 22 April 2002

Abstract

Theoretical cell model is applied for evaluation of valve-regulated lead–acid batteries under discharge, recharge and overcharge conditions. The previously presented models are improved by introducing a new formula for electrode morphology, applying charging factor to state-of-charge, electrode porosity and acid concentration as well as considering the recombination of oxygen as mass-transport limited evolution process. Also, a new model is proposed for the ohmic resistance of a battery. The modified cell model is calibrated using experimental data. Results show that high prediction accuracy can be obtained for the full discharge–recharge cycle including deep discharge and overcharge. The modified cell model is applied for evaluation of the gas formation processes using externally measured current, voltage and temperature of a battery.

Keywords: Modelling; Simulation; State estimation; State-of-health; VRLA battery

1. Introduction

The purpose of the paper is to propose a model for overcharging of a battery. The model covers the full discharge–recharge cycle including deep discharge and overcharge. The model is an extension of previously presented model [19] that is modified by developing new formula for electrode morphology, applying charging factor to state-of-charge, electrode porosity and acid concentration as well as considering the recombination of oxygen as mass-transport limited evolution process and other.

Uninterruptible power supply (UPS) systems are used to power telecom switching systems that contain ac/dc power supplies and storage batteries connected in parallel. Valve-regulated lead–acid (VRLA) battery technologies are typically used. The life expectancy of VRLA batteries has turned out to be much shorter and more unpredictable than expected necessitating the use of proper battery monitoring equipment. Total uninterruptibility of operation is required. This means that the conditional monitoring of a battery cannot be based on extensive discharging due to increased risk of down time, even if it is considered as the only reliable method to assess the state-of-health.

Many attempts have been made to find a reliable method to assess the state-of-health without discharging battery. Impedance or conductance of a battery has been proposed as a viable candidate for this purpose but has turned out not to contain the information required [12]. If the requirement of discharging can be somewhat relaxed, i.e. a short discharge of 10–20% of total capacity is allowed then a more complex theoretical cell model may be used in assessing the state-of-health. It has turned out that a short discharge, and the subsequent recharging up to the overcharge may provide the information needed for the accurate prediction of discharge behaviour of a battery and its state-of-health. The key is the overcharge process that is considered in more detail in this paper.

The history of modelling of a lead–acid battery dates back to the late 1950s. A good review of the development in the theory of flooded porous electrodes prior to 1975 can be found, e.g. in [15]. Many researchers have made improvements in the modelling. As a result quite complete model was developed as described in [8,17,20]. This model was later extended to 2D-model [2,5,9]. From the overcharging point of view the following two improvements are significant.

1. *Two-step reaction*: It is shown in [7,18] that the dissolution process is the rate limiting factor at higher

* Corresponding author.
E-mail address: ander.tenno@hut.fi (A. Tenno).

0378-7753/02/$ – see front matter
PII: S0378-7753(02)00276-8

Nomenclature

A_{H_2}	active surface area for hydrogen reaction (cm^2/cm^3)
A_{max}	maximum active surface area (cm^2/cm^3)
A_M	active surface area for primary reaction (cm^2/cm^3)
A_{O_2}	active surface area for oxygen reaction (cm^2/cm^3)
c	acid concentration (mol/cm^3)
c_{Pb_2}	concentration of lead ions
$c^*_{Pb_2}$	saturation constant
c_{ref}	electrolyte initial concentration (mol/dm^3)
D	electrolyte diffusion constant (cm^2/s)
E_A	activation energy (kJ/mole)
f	molar activity coefficient
F	Faraday's constant (C/mol)
g_j	electrode resistance of single layer (Ω)
h	layer thickness (cm)
i	current density in electrolyte (A/cm^2)
i_{app}	applied current (A)
$i^{H_2}_{app}$	applied current for hydrogen reaction (A)
i^{M}_{app}	applied current for primary reaction (A)
$i^{O_2}_{app}$	applied current for oxygen reaction (A)
i_k	current density of positive or negative electrode through single layer (A/cm^2)
i_{H_2}	current density generated by hydrogen reaction (A/cm^2)
i_M	current density generated by primary reaction (A/cm^2)
i_{O_2}	current density generated by oxygen reaction (A/cm^2)
$i^{H_2}_0$	exchange current density for hydrogen reaction (A/cm^2)
i^{M}_0	exchange current density for primary reaction (A/cm^2)
$i^{O_2}_0$	exchange current density for oxygen reaction (A/cm^2)
I_{PbSO_4}	limit current density for cathodic reaction (A/cm^2)
j_{H_2}	transfer current density for hydrogen reaction (A/cm^2)
j_M	transfer current density for primary reaction (A/cm^2)
j_{O_2}	transfer current density for oxygen reaction (A/cm^2)
k_{ore}	oxygen recombination efficiency
$k^{H_2}_m$	heat flux density for hydrogen reaction (mW/cm^2)
$k^{O_2}_m$	heat flux density for oxygen reaction (mW/cm^2)
k_{PbSO_4}	mass-transfer coefficient for lead ions (cm/s)
K_1	equivalent volume to charge constant (cm^3/C)
K_2	equivalent molarity to charge constant
K_3	absolute constant (mol/C)
n_{H_2}	number of moles of hydrogen generated on negative electrode (mol)
n_{O_2}	number of moles of oxygen generated or reduced on electrode (mol)
$n^g_{O_2}$, $n^g_{H_2}$	number of gas moles of oxygen or hydrogen accumulated in the free space of battery (mol)
n_{H_2O}	number of water moles (mol)
p_{H_2}	hydrogen partial pressure (Pa)
p_{O_2}	oxygen partial pressure (Pa)
$p^{ref}_{O_2}$, $p^{ref}_{H_2}$	reference value of partial pressure of oxygen or hydrogen (Pa)
p_i	electrolyte resistance of single layer (Ω)
Q_0	oxygen flow velocity through separator (cm/s)
Q_{max}	theoretical capacity of electrode (C/cm^3)
Q_{Joule}	heat (J)
r_i	charge-transfer resistance of single layer (Ω)
R	universal gas constant (J/mol K)
R_{bat}	battery ohmic resistance (Ω)
R_{H_2}	charge-transfer resistance of electrode for hydrogen reaction (Ω)
R_M	charge-transfer resistance of electrode for primary reaction (Ω)
R_{O_2}	charge-transfer resistance of electrode for oxygen reaction (Ω)
R_{cell}	cell resistance (Ω)
R^+_n	positive electrode resistance (Ω)
R^-_n	negative electrode resistance (Ω)
R_{acid}	electrolyte resistance in electrodes or separator (Ω)
R_{cond}	resistance of battery conducting elements (Ω)
R_{sep}	electrolyte resistance in separator (Ω)
S	gross-section area of electrode (plate area) (cm^2)
t^0_+	transference number
T	temperature (K)
T_0	298.2 K—standard temperature, i.e. 25 °C
u	float voltage (per cell) (V)
U	thermodynamic equilibrium potential for primary reaction (V)
U_{H_2}	thermodynamic equilibrium potential for hydrogen reaction (V)
U_{O_2}	thermodynamic equilibrium potential for oxygen reaction (V)
v	voltage drop due to applied current (V)
w	polarization (V)

Greek letters

α_{Ah}	charging efficiency
α_a	anodic apparent transfer coefficient for primary reaction
α_c	cathodic apparent transfer coefficient for primary reaction
$\alpha^{H_2}_c$	apparent transfer coefficient for hydrogen reaction
α_{O_2}	apparent transfer coefficient for oxygen reaction

β	tortuosity exponent
γ, ρ	electrode morphology coefficients
ε	porosity
η	surface overpotential for primary reaction (V)
η_{H_2}	surface overpotential for hydrogen reaction (V)
η_{O_2}	surface overpotential for oxygen reaction (V)
θ	state-of-charge
κ	acid conductivity (S/cm)
σ_{bulk}	conductivity of bulk electrode (S/cm)
ϕ^s	solid matrix potential (V)
ϕ^l	electrolyte potential (V)

overvoltage, and the diffusion rate is limiting factor at lower overvoltage, respectively. A new dissolution-electrode reaction model was proposed including the effect of state-of-charge. This model was applied to the prediction of a cell behaviour in [13] demonstrating a good fit of model and experiment for acid concentration and porosity of electrodes.

2. *Overcharging*: The latest progress has been made in description of the behaviour of a battery under float charging. The gas formation process of VRLA batteries has been analysed in [3,4] using simple lumped parameter model of the behaviour of battery under float charging. This model was thoroughly tested experimentally. The gas formation processes were also analysed in [1] with a distributed parameter model and in [11] with a 2D-model. It is suggested in [15] that the dissolution-limited electrode reaction model, proposed in [18], could improve the accuracy of the model. They show somewhat better accuracy of model against measured data provided in [1]. Regardless of suggested model, even better accuracy is shown in [10] on the same set of data using simple single-step reaction model but with different function for electrode morphology. The latter model is tested on a new set of data in [14], showing less agreement of the model with measured data during overcharging.

Accuracy and reliability of the proposed models are not high for overcharging. They have only been tested in a few experiment. This work is continued in this paper on a new set of experimental data with improved model. The following changes are introduced in the proposed earlier models [1,16].

1. The battery model is modified with respect to electrode morphology. The charging factor is applied in state-of-charge, electrode porosity and acid concentration models. Mass transport of oxygen through separator is considered in more detail. The recombination of oxygen is considered as a mass-transport limited evolution process. The model for battery ohmic resistance is proposed and applied to voltage drop prediction.
2. It is shown that the theoretical cell model can be simplified when applied to battery testing. The single-step reaction model has the same prediction accuracy as the two-step reaction model. The partial pressure of gases can be eliminated from the electrode reaction equation using preset pressure window for valve.
3. The model is calibrated using experimental data in respect to gas formation processes.
4. High prediction accuracy of the model is demonstrated in a wide range of charge–discharge processes, including deep discharge and overcharge. It is shown that different behaviour of individual batteries in series during the overcharge can be predicted.
5. The model is applied to the unobservable gas formation processes in the battery. Oxygen evolution and recombination processes and water dry-out are evaluated during discharge, recharge and overcharge.
6. Model for the ohmic resistance is proposed based on the charge-transfer resistances for the primary reaction and gassing reaction. The ohmic resistance is different for charge, discharge and overcharge processes—it depends strongly on the state-of-charge of the battery.
7. It is shown that high charge-transfer resistance can explain the high float voltage during overcharge but there is no direct link between the overcharge voltage and the battery capacity.

The following conventional reaction schemes of VRLA battery are considered in this paper.

Positive electrode: primary reaction: charge or discharge

$$PbSO_4 + 2H_2O \Leftrightarrow PbO_2 + HSO_4^- + 3H^+ + 2e^-,$$

oxygen evolution

$$2H_2O \rightarrow O_2 + 4H^+ + 4e^-,$$

grid corrosion

$$Pb + 2H_2O \rightarrow PbO_2 + 4H^+ + 4e^-,$$

Negative electrode: primary reaction: charge or discharge

$$PbSO_4 + H^+ + 2e^- \Leftrightarrow Pb + HSO_4^-,$$

oxygen reduction

$$O_2 + 4H^+ + 4e^- \rightarrow 2H_2O,$$

hydrogen evolution

$$2H^+ + 2e^- \rightarrow H_2.$$

The oxygen evolution and reduction processes are well-balanced by the special design of VRLA battery.

2. Model

The charge–discharge behaviour of a battery depends on electrode kinetics affected by the electrode potential in solid matrix and electrolyte, electrode porosity, and the acid density in pores of electrode. The electrode kinetics are different for the primary reaction and gassing reactions. The basic model developed for lead–acid cell by White,

Newman, Simonsson and other authors is analysed and modified in this section.

2.1. Electrode kinetics

The electrode reaction current is related to the material of the electrode (lead or lead dioxide) and electrolyte (water and sulphuric acid) as follows:

$$\frac{\partial i}{\partial x} = \frac{\partial i_{\mathrm{M}}}{\partial x} + \frac{\partial i_{\mathrm{O_2}}}{\partial x} + \frac{\partial i_{\mathrm{H_2}}}{\partial x}, \tag{1}$$

where i is the current density in the liquid phase in pores of electrode (A/cm^2) and i_{M} is the current density generated by primary reaction with lead or lead dioxide (A/cm^2)

$$\frac{\partial i_{\mathrm{M}}}{\partial x} = A_{\mathrm{M}} j_{\mathrm{M}},$$

where A_{M} is the active surface area per unit volume of porous electrode (cm^2/cm^3), j_{M} the transfer current density for primary reaction (A/cm^2), $A_{\mathrm{M}} j_{\mathrm{M}}$ the volumetric reaction rate (A/cm^3) and $i_{\mathrm{O_2}}$ is the current density generated by oxygen reaction,

$$\frac{\partial i_{\mathrm{O_2}}}{\partial x} = A_{\mathrm{O_2}} j_{\mathrm{O_2}},$$

where $A_{\mathrm{O_2}}$ is the active surface area for oxygen reaction, $j_{\mathrm{O_2}}$ the transfer current density for oxygen reaction and $i_{\mathrm{H_2}}$ is the current density generated by hydrogen reaction,

$$\frac{\partial i_{\mathrm{H_2}}}{\partial x} = A_{\mathrm{H_2}} j_{\mathrm{H_2}},$$

where $A_{\mathrm{H_2}}$ is the active surface area for hydrogen reaction and $j_{\mathrm{H_2}}$ the transfer current density for hydrogen reaction.

2.1.1. Surface area

The active surface area between solid and liquid phases depends on the utilisation of the electrode. The surface area in discharge and recharge reactions can be estimated as

1. Primary reaction

$$A_{\mathrm{M}} = A_{\max} \frac{\rho}{\exp(\gamma\theta)} \quad \text{(recharge)}, \tag{2}$$

$$A_{\mathrm{M}} = A_{\max} \theta^{\beta_1} \quad \text{(discharge)}. \tag{3}$$

2. Oxygen and hydrogen reactions (for both discharge and recharge)

$$A_{\mathrm{O_2}} = A_{\mathrm{H_2}} = A_{\max} \theta^{\beta_1}.$$

where $A_{\max}$ is the maximum active surface area (cm^2/cm^3), ρ, γ the electrode morphology coefficients, β_1 the tortuosity exponent and θ is the state-of-charge (SOC).

The exponential function (2) can predict the surface area rather precisely as shown in [19] where the simplified (2) and exact formulas were introduced and compared. The exact formula

$$A_{\mathrm{M}} = \rho A_{\max} \frac{\exp(\gamma - \gamma\theta) - 1}{\exp(\gamma) - 1},$$

is more useful for overcharging. It has better asymptotic properties for $\theta \to 1$.

The state-of-charge is defined as a charge fraction from theoretical capacity

$$\frac{\partial \theta}{\partial t} = \frac{\alpha_{\mathrm{Ah}}}{Q_{\max}} \frac{\partial i}{\partial x},$$

where $Q_{\max}$ is the theoretical capacity (C/cm^3) and α_{Ah} is the charging efficiency.

The charging efficiency is defined for charging process as the ratio between required charge (Ah) and available capacity (Ah). It improves the model accuracy. A local loss of accuracy is small (3–6%) per single step but it accumulates during recharge process if this parameter is ignored (total loss is large). This simple fact has not been recognised properly in the literature.

The state-of-charge is always lower than the one calculated based on pure current due to heat generation (Joule effect) and dissipation, current losses through isolation and battery gassing.

Some parameters cannot be identified uniquely and they are reduced from model. For example, the exchange current density and maximum surface area cannot be estimated as independent parameters using the current–voltage and temperature measurements. They are considered as a total parameter or product of the exchange current density and maximum surface area. If one of them is chosen as a constant using the values presented in the literature then another can be estimated from data. If the maximum surface area is chosen as a constant then the same constant can be applied for oxygen, hydrogen and primary reactions. The exchange current densities of these reactions can be estimated uniquely from measured data. The number of estimated parameters of model is minimised.

2.1.2. Single-step reaction

The volumetric reaction rate depends on overpotential as a two-directional process. Both processes, anodic and cathodic, are limited by acid concentration

$$j_{\mathrm{M}} = i_0^{\mathrm{M}} \left(\frac{c}{c_{\mathrm{ref}}}\right)^{\beta_2} \left[\exp\left(\alpha_{\mathrm{a}} \frac{F}{RT}\eta\right) - \exp\left(-\alpha_{\mathrm{c}} \frac{F}{RT}\eta\right)\right], \tag{4}$$

where i_0^{M} is the exchange current density for standard temperature of 25 °C (A/cm^2), c the acid concentration (mol/cm^3), c_{ref} the initial concentration (reference value) (mol/dm^3), β_2 the tortuosity exponent, η the surface overpotential ($\eta = \phi^{\mathrm{l}} - \phi^{\mathrm{s}} - U$), $\phi^{\mathrm{l}} - \phi^{\mathrm{s}}$ the electrode polarisation (V), ϕ^{s} the solid matrix potential (V), ϕ^{l} the electrolyte potential (V), U the thermodynamic equilibrium potential (V), α_{a} the anodic apparent transfer coefficient, α_{c}

the cathodic apparent transfer coefficient ($\alpha_c = 2 - \alpha_a$), T the temperature (K), R the universal gas constant and F is the Faraday's constant.

Thermal relationship: The exchange current density depends on temperature. The following formula can be used for correction of the exchange current density in a wide temperature range [4]

$$i_0^M(T) = i_0^M \exp\left\{\frac{E_A(T - T_0)}{RT_0T}\right\}, \quad (5)$$

where E_A is the activation energy, $E_A = 50$ kJ/mole, $T_0 = 298.2$ K—standard temperature, i.e. 25 °C.

This simplest reaction rate equation is adequate description of the charge–discharge behaviour of a battery under high or medium charging rates. A more complex two-step reaction model was suggested in [6,18] and later in [16] for the batteries under low charging rate.

2.1.3. Two-step reaction

The dissolution of sulphate crystals and formation of lead ions in solution is limited by solubility. The dissolution transfer current density is equal to

$$j_M = 2Fk_{PbSO_4}(c_{Pb_2} - c^*_{Pb_2}), \quad (6)$$

where c_{Pb_2} is the concentration of lead ions, $c^*_{Pb_2}$ the saturation concentration and k_{PbSO_4} is the mass-transfer coefficient for lead ions (cm/s).

The diffusion of lead ions from solution into the lead is limited by ions concentration. The diffusion transfer current density is equal to

$$j_M = i_0^M\left(\frac{c}{c_{ref}}\right)^{\beta_2}\left[\exp\left(\alpha_a\frac{F}{RT}\eta\right) - \frac{c_{Pb_2}}{c^*_{Pb_2}}\exp\left(-\alpha_c\frac{F}{RT}\eta\right)\right]. \quad (7)$$

Partially, this is similar to the single-step reaction model but the cathodic reaction is dissolution-limited.

2.1.3.1. Two-step reaction model. Dependence on the lead ions can be eliminated from Eq. (7) using equality between dissolution (6) and diffusion (7) current densities. The two-step reaction model can be expressed as

$$j_M = i_0^M\left(\frac{c}{c_{ref}}\right)^{\beta_2} I_{PbSO_4}\left\{\exp\left[(\alpha_a + \alpha_c)\frac{F}{RT}\eta\right] - 1\right\} \times \left\{i_0^M\left(\frac{c}{c_{ref}}\right)^{\beta_2} + I_{PbSO_4}\exp\left(\alpha_c\frac{F}{RT}\eta\right)\right\}^{-1}, \quad (8)$$

where I_{PbSO_4} is the limit current density for cathodic reaction (A/cm^2)

$$I_{PbSO_4} = 2Fk_{PbSO_4}c^*_{Pb_2}.$$

Its value is higher by an order of magnitude for positive electrode. The mass-transfer of lead ions into solution is much faster at positive electrode than at negative electrode.

The two-step reaction model is assumed, as in [16], to be suitable model for negative electrode and single-step reaction model for positive electrode. However, this was not confirmed based on experiment (Section 3). Nearly equal accuracy was achieved experimentally for both reaction models. A simpler single-step reaction model is suggested in this paper.

2.1.4. Oxygen reaction

The transfer current density for oxygen reaction depends on overpotential as a two-directional process. Both processes, anodic and cathodic, are limited by acid concentration. The cathodic reaction is limited by the partial pressure of oxygen [16]

$$j_{O_2} = i_0^{O_2}\left(\frac{c}{c_{ref}}\right)^{\beta_3} \times \left[\exp\left(\alpha_{O_2}\frac{F}{RT}\eta_{O_2}\right) - \left(\frac{p_{O_2}}{p^{ref}_{O_2}}\right)^{\beta_4}\exp\left(-\alpha_{O_2}\frac{F}{RT}\eta_{O_2}\right)\right], \quad (9)$$

where $i_0^{O_2}$ is the exchange current density for oxygen reaction, β_3, β_4 the tortuosity exponents, η_{O_2} the surface overpotential for oxygen reaction ($\eta_{O_2} = \phi^l - \phi^s - U_{O_2}$), U_{O_2} the thermodynamic equilibrium potential for oxygen, α_{O_2} the apparent transfer coefficient for oxygen, p_{O_2} the oxygen partial pressure (Pa) and $p^{ref}_{O_2}$ is the reference pressure.

This model is close to the earlier presented in [1] model and obtained by eliminating the partial pressure from anodic reaction.

Thermal relationship: The exchange current density can be corrected using (5) when the temperature deviates from the standard temperature. The activation energy is higher ($E_A = 69$ kJ/mole) for oxygen reaction than for primary reaction [4].

2.1.4.1. Oxygen evolution. The electrode potential $U = 1.75$ V on positive electrode is shifted far over the equilibrium potential ($U_{O_2} = 1.23$ V) for oxygen. The current density for cathodic reaction is essentially lower than for anodic reaction because of shifted potential (0.52 V) to higher values. The cathodic reaction can be ignored on positive electrode. The oxygen evolution can be predicted as a single-directional anodic reaction on positive electrode that is not limited by partial pressure of oxygen

$$j_{O_2} = i_0^{O_2}\left(\frac{c}{c_{ref}}\right)^{\beta_3}\exp\left(\alpha_{O_2}\frac{F}{RT}\eta_{O_2}\right). \quad (10)$$

The reduction rate depends on oxygen transfer through separator and on oxygen recombination rate on negative electrode.

2.1.4.2. Oxygen reduction. The electrode potential of $U = -0.32$ V on negative electrode is shifted far below the equilibrium potential for oxygen ($U_{O_2} = 1.23$ V). The

recombination process is a single-directional cathodic reaction of (9) in this case

$$j_{O_2} = -i_0^{O_2}\left(\frac{c}{c_{ref}}\right)^{\beta_3}\left(\frac{p_{O_2}}{p_{O_2}^{ref}}\right)^{\beta_4}\exp\left(-\alpha_{O_2}\frac{F}{RT}\eta_{O_2}\right). \quad (11)$$

This is a very fast process because of shifted potential of 1.55 V to lower values. It is mainly limited by oxygen transport through separator and slightly by oxygen partial pressure. The latter limitation is insignificant and can be ignored. The oxygen partial pressure is close to reference pressure $p_{O_2}^{ref}$ under correctly operating valves. The gas pressure is limited in a narrow band within the preset pressures between the opening pressure and the closing pressure of the valve. The gas content is stable—90% hydrogen and 10% oxygen, as is the partial pressure for both gases.

Another recombination model suggested in [16] assumes no oxygen transfer through separator and consequently no reduction without oxygen partial pressure. The recombination process depends on mass-transfer and oxygen pressure but is independent of electrode potential

$$j_{O_2} = -4k_m^{O_2}\frac{F}{RT}p_{O_2}, \quad (12)$$

where $k_m^{O_2}$ is the heat flux density (mW/cm^2).

However, it is unrealistic to assume in (12) that low partial pressure can control the recombination process so well that the usual recombination efficiency (99%) can be obtained. The oxygen volumetric concentration is rather low in exhaust gases (less than 10%). The oxygen evolution and recombination current varies in a wide range during recharge. Anyway, they are close to each other because of high recombination efficiency. Therefore, large variations of partial pressure of oxygen should be concluded from the model (12) which has been not reported in the literature.

Probably, the variation of the partial pressure is relatively slow. It is an integrated value over certain accumulation period (several hours) for gases in free space of battery head. Both slow variation and low partial pressure fail to explain high recombination efficiency in either of the models (11) or (12).

It is much more practical to evaluate the recombination rate proportionally to evolution rate and mass transport rate through separator than to do it by partial pressure of oxygen. The following mass-transfer and recombination model is proposed and verified in this paper.

2.1.4.3. Oxygen transfer. The oxygen transfer through separator is evaluated by a simple mass-transfer model

$$\frac{\partial i_{O_2}}{\partial t} = Q\frac{\partial i_{O_2}}{\partial x}, \qquad i_{O_2}(x_{p/s}) = i_{O_2}(x_{p/s}), \quad (13)$$

where Q is the oxygen flow velocity through separator (cm/s) and $i_{O_2}(x_{p/s})$ is the current density at the boundary between positive electrode and separator.

In general, the flow velocity depends on partial pressure. A linear function $Q = Q_0 p_{O_2}/p_{O_2}^{ref}$ can be used to approximate this relationship. Approximation with constant flow velocity $Q = Q_0$ is a practical approach resulting from constant partial pressure under normal operating conditions of valves. This practical approach was used in analysis of test batteries.

The current density at the boundary between positive electrode and separator can be calculated as a boundary value solution of Eq. (10).The oxygen transfer in separator can be the rate-limiting step in the case of rapid changes in the evolution of oxygen on positive electrode. A transport-delay through separator is observable as a shock wave is the consequence of rapid change of oxygen evolution. This wave can be predicted by the model (13).

2.1.4.4. Oxygen recombination. The oxygen mass-transfer and reduction on negative electrode is proposed to be evaluated as follows:

$$\frac{\partial i_{O_2}}{\partial t} = Q_0\frac{\partial i_{O_2}}{\partial x} + k_{ore}A_{O_2}j_{O_2}, \qquad i_{O_2}(x_{s/n}) = i_{O_2}(x_{s/n}), \quad (14)$$

where k_{ore} is the oxygen recombination efficiency (ORE), j_{O_2} the transfer current density on negative electrode for oxygen reaction, calculated by single-directional (11) or two-directional process model (9) using reference pressure $p_{O_2} = p_{O_2}^{ref}$, A_{O_2} is the active surface area of negative electrode and $i_{O_2}(x_{s/n})$ is the current density at boundary between separator and negative electrode, calculated as a solution of Eq. (13) at boundary.

Penetration of oxygen is not deep in negative electrode. The reduction rate is fast because of shifted potential, there is not much oxygen penetrated under the surface layer of negative electrode.

Steady-state model: A simple and useful model is the following recombination model for steady-state reaction

$$j_{O_2}^- = -j_{O_2}^+ k_{ore}\frac{A_{O_2}^+}{A_{O_2}^+}. \quad (15)$$

In this model the volumetric reaction rate for recombination is considered proportional to the evolution rate $A_{O_2}^- j_{O_2}^- = -k_{ore}A_{O_2}^+ j_{O_2}^+$. The transfer current density for recombination process is proportional to the transfer current density for the evolution process.

The steady-state oxygen recombination process with constant ORE can be evaluated by this reduced order model (15). More general oxygen recombination process with variable ORE should be evaluated by the dynamic models of (9) and (14). The oxygen mass-transfer is limited or delayed in the case of rapid changes in the applied current.

2.1.4.5. Applied model. The two-directional reaction model of (9) is used for experimental data analysis in Section 3. It is assumed that the oxygen partial pressure is close to the

reference pressure. The exchange current density is corrected using (5) with measured temperature. The oxygen transfer through separator is estimated by the mass-transfer model of (13) and the oxygen recombination by the steady-state process model of (15).

2.1.5. Hydrogen reaction

The transfer current density for hydrogen reaction depends on overpotential as a two-directional process. Both processes, anodic and cathodic, are limited by acid concentration. The anodic reaction is limited by the partial pressure of hydrogen

$$j_{H_2} = i_0^{H_2}\left(\frac{c}{c_{ref}}\right)^{\beta_5} \times \left[\left(\frac{p_{H_2}}{p_{H_2}^{ref}}\right)^{\beta_6}\exp\left(\alpha_{H_2}\frac{F}{RT}\eta_{H_2}\right) - \exp\left(-\alpha_{H_2}\frac{F}{RT}\eta_{H_2}\right)\right], \quad (16)$$

where $i_0^{H_2}$ is the exchange current density for hydrogen reaction, β_5, β_6 the tortuosity exponent, η_{H_2} the surface overpotential for hydrogen reaction ($\eta_{H_2} = \phi^l - \phi^s - U_{H_2}$), U_{H_2} the thermodynamic equilibrium potential for hydrogen, α_{H_2} the apparent transfer coefficient for hydrogen, p_{H_2} the hydrogen partial pressure (Pa) and $p_{H_2}^{ref}$ is the reference pressure.

This model is similar to the oxygen reaction model of (9) modified for the hydrogen reaction.

Hydrogen pressure: The hydrogen partial pressure is close to reference pressure $p_{H_2} = p_{H_2}^{ref}$ under correctly operating valves.

Thermal relationship: The exchange current density can be corrected using (5) when the temperature deviates from the standard temperature. The activation energy is lower ($E_A = 54$ kJ/mole) for hydrogen reaction than for oxygen reaction [4].

2.1.5.1. Hydrogen evolution.

The electrode potential $U = -0.35$ V on negative electrode is shifted far below equilibrium potential ($U_{H_2} = 0$ V) for hydrogen. The hydrogen evolution can be predicted as a single-directional cathodic process on negative electrode [16]

$$j_{H_2} = -i_0^{H_2}\left(\frac{c}{c_{ref}}\right)^{\beta_5}\exp\left(-\alpha_{H_2}\frac{F}{RT}\eta_{H_2}\right). \quad (17)$$

Steady-state model: The following steady-state reaction model is a simple hydrogen evolution model

$$j_{H_2}^- = -j_{O_2}^+(1 - k_{ore})\frac{A_{O_2}^+}{2A_{H_2}^-}. \quad (18)$$

The evolution rate of hydrogen is proportional to the imbalance between oxygen evolution and recombination rates $2A_{H_2}^- j_{H_2}^- = A_{O_2}^+ j_{O_2}^+ + A_{O_2}^- j_{O_2}^-$ or to the oxygen evolution rate $2A_{H_2}^- j_{H_2}^- = (k_{ore} - 1)A_{O_2}^+ j_{O_2}^+$. The hydrogen evolution transfer current density is proportional to the oxygen evolution transfer current density.

The hydrogen evolution can be evaluated using the steady-state model of (18) in the case of constant ORE. More general dynamic model (16) should be used in the case of variable ORE.

The hydrogen evolution is much smaller ($1 - k_{ore} = 10^{-2}$ times) than oxygen evolution. Its real effect on overall current (1) is insignificant if compared with oxygen evolution or recombination current.

2.1.5.2. Hydrogen reduction.

A similar model to (12) was proposed for hydrogen recombination in [16]. No hydrogen transfer through separator and consequently no recombination without hydrogen partial pressure was assumed. The recombination process depends on mass-transfer and hydrogen pressure but is independent of electrode potential

$$j_{H_2} = -2k_m^{H_2} p_{H_2},$$

where $k_m^{H_2}$ is the heat flux density (mW/cm^2).

It is extremely difficult to measure the real hydrogen recombination rate experimentally. A small recombination rate is expected according to a consistent model.

2.1.5.3. Hydrogen recombination.

The hydrogen recombination process on positive electrode is far too slow and can be ignored [3]. It is much slower than could be expected by single-directional anodic process for potential of 1.75 V that is far shifted over zero equilibrium potential for hydrogen. A slow recombination process is in good agreement with measurements but not with potential. The hydrogen content is about 90% of exhaust gases.

A similar model to the oxygen recombination process of (14) can be used for the hydrogen recombination process but with much lower recombination efficiency ($\eta_{ore} < 0.1$). As a result, a simple process like transport of hydrogen through separator into positive electrode can be simulated with this model but is insignificant for battery analysis.

2.1.5.4. Applied model.

The two-directional reaction model of (16) is used for experimental data analysis in Section 3. It is assumed that hydrogen partial pressure is close to reference pressure. The exchange current density for standard temperature is corrected using (5) with measured temperature. Zero recombination process at positive electrode is assumed.

2.2. Potential in solid matrix

The conductivity of bulk electrodes is high: 0.5 kS/cm for positive electrode and 48 kS/cm for negative electrode. The voltage drop on solid matrix is 10^4 times smaller than voltage drop on electrolyte for positive electrode and 10^6 times less for negative electrode. The voltage drop is almost

zero on solid matrix of porous electrode. It is especially low in the case of float charging with low rate. The voltage drop on solid matrix can be ignored or considered as a small component of polarisation (Section 2.6).

2.3. Potential in electrolyte

Ohm's law for solution relates the current and potential in electrolyte

$$\frac{i}{\kappa^{\text{eff}}} = -\frac{\partial\phi^1}{\partial x} + \frac{RT}{F} + (1-2t_+^0)\frac{\partial \ln fc}{\partial x},$$

where i is the current density in electrolyte (A/cm^2), ϕ^1 the potential in electrolyte (V), κ^{eff} the conductivity of porous electrodes or separator, $\kappa^{\text{eff}} = \kappa\varepsilon^{\beta_7}$, κ the acid conductivity (S/cm), ε the porosity, β_7 the tortuosity exponent, t_+^0 the transference number and f is the molar activity coefficient.

2.4. Electrode porosity

The electrode volume fraction filled with electrolyte can be evaluated as

$$\frac{\partial\varepsilon}{\partial t} = K_1\alpha_{\text{Ah}}\frac{\partial i}{\partial x}, \tag{19}$$

where ε is the porosity, α_{Ah} the charging efficiency and K_1 is the equivalent volume to charge constant (cm^3/C).

The electrode porosity is not affected by current for heat generation (Joule effect) and dissipation. This current is eliminated from (19) using charging efficiency factor.

2.5. Acid concentration

The acid concentration depends on migration and diffusion of species. The migration is induced as ion current by primary reaction and oxygen, hydrogen reactions. The diffusion is induced by concentration gradient which is largest between positive electrode and separator

$$\varepsilon\frac{\partial c}{\partial t} = \frac{\partial D^{\text{eff}}}{\partial x}\frac{\partial c}{\partial x} + (K_2 - cK_1)\alpha_{\text{Ah}}\frac{\partial i}{\partial x} + K_3\left(\frac{\partial i_{\text{O}_2}}{\partial x} + \frac{\partial i_{\text{H}_2}}{\partial x}\right), \tag{20}$$

where c is the acid concentration (mol/cm^3), D^{eff} the diffusion in porous electrodes or separator ($D^{\text{eff}} = D\varepsilon^{\beta_8}$), D the electrolyte diffusion constant (cm^2/s), ε the porosity, β_8 the tortuosity exponent, α_{Ah} the charging efficiency and K_2 is the equivalent molarity to charge constant (mol/C)

$$K_2^+ = \frac{(3-2t_+^0)}{2F}, \qquad K_2^- = \frac{(1-2t_-^0)}{2F},$$

K_3 is the absolute constant (mol/C), $K_3^+ = -K_3^- = (2F)^{-1}$.

The ion migration due to water decomposition is accounted for in (20). The acid concentration is not affected by current for heat generation and dissipation. This current is eliminated from (20) using charging efficiency factor.

2.6. Resistance

Current flow through surface area of electrode (interface between electrode and electrolyte), generates heat proportional to the voltage drop caused by reaction hindrance [3]

$$\frac{\mathrm{d}Q_{\text{Joule}}}{\mathrm{d}t} = \eta i_{\text{app}}, \tag{21}$$

where Q_{Joule} is the heat (J), η the overvoltage of single electrode (V) and i_{app} is the applied current (A).

This heat is equal to the same amount of heat generated by the current flow through equivalent ohmic resistance

$$\frac{\mathrm{d}Q_{\text{Joule}}}{\mathrm{d}t} = i_{\text{app}}^2 R, \tag{22}$$

where R is the ohmic resistance of single electrode (W).

2.6.1. Charge-transfer resistance

The charge-transfer resistance can be calculated as ohmic resistance from heat equality (21) and (22) as

$$R = \frac{\eta}{i_{\text{app}}}. \tag{23}$$

This is similar to Ohm's law but the voltage drop is considered as the deviation from the equilibrium potential, and the resistance depends on direction of the applied current: the charge-transfer resistance is different for discharge and recharge reactions.

2.6.2. Local resistance

The charge-transfer resistance can be calculated as a local parameter for every layer in the electrode

$$r_i = \frac{\eta_i}{A_i j_i h S}, \tag{24}$$

where r_i is the charge-transfer resistance of layer, $r_i = r(x_i)$ (Ω), $\eta(x_i)$ the overpotential of layer ($\eta_i = \eta(x_i)$) (V), A_i the active surface area of layer ($A_i = A(x_i)$) (cm^2/cm^3), j_i the transfer current density of layer ($j_i = j(x_i)$) (A/cm^2), h the layer thickness (cm) and S is the gross-section area of electrode (cm^2).

2.6.3. Cell resistance

The cell resistance is equal to the overall charge-transfer resistance in both electrodes, and to the electrolyte resistance in separator and in pores of electrodes

$$R_{\text{cell}} = R_n^+ + R_n^- + R_{\text{sep}}, \tag{25}$$

where R_{cell} is the cell resistance (Ω), R_n^+ the positive electrode resistance, R_n^- the negative electrode resistance and R_{sep} is the electrolyte resistance in separator.

The electrode resistance can be calculated as a sum R_n of local charge-transfer resistances for every layer connected in parallel and electrolyte resistances connected in series

(resistance on solid matrix of electrode is ignored in this formula)

$$R_i = p_i + \frac{r_i R_{i-1}}{r_i + R_{i-1}}, \qquad R_0 = p_0 + r_0, \quad i = 1, \ldots, n, \tag{26}$$

where r_i is the charge-transfer resistance and p_i is the electrolyte resistance of single layer.

The electrolyte resistance can be calculated as a sum of single layer resistances over separator

$$R_{\text{sep}} = \sum_{i=0}^{n} p_i^{\text{sep}}. \tag{27}$$

The electrolyte single layer resistance $p_i = p(x_i)$ can be calculated using the conductivity of layers in positive or negative electrodes, or in separator using the relationship

$$p_i = \frac{h}{\kappa(c_i, T)\varepsilon_i S}. \tag{28}$$

The electrolyte conductivity κ depends on acid concentration $c_i = c(x_i)$ and temperature. It can be evaluated using the empirical formula $\kappa(c_i, T)$ suggested in [15]. The volume fraction filled with acid in electrodes and separator is accounted for through porosity $e_i = e(x_i)$ in (28).

The conductivity of solid matrix of electrodes was ignored in (26). If it were accounted for, the calculation formula would be more complicated. The electrode resistance can be calculated as a sum R_n of local charge-transfer resistances for every layer connected in parallel and electrolyte resistances and solid matrix resistances connected in series (Fig. 1)

$$R_n = T_n^{-1} + \sum_{i=1}^{n-1} L_i^{-1}(P_{i-1} + p_i)(G_{i-1} + g_i),$$

where

$$T_n = (P_{n-1} + p_n)^{-1} + (G_{n-1} + g_n)^{-1},$$
$$L_i = P_{i-1} + p_i + G_{i-1} + g_i + r_i,$$

P_i, B_i, $i = 1, 2, \ldots, n-1$ are defined as solution of the system

$$P_i = S_i^{-1}(P_{i-1} + p_i)r_i, \quad P_0 = 0,$$
$$G_i = S_i^{-1}(G_{i-1} + g_i)r_i, \quad B_0 = r_0.$$

The resistance of porous electrode depends on solid matrix volume fraction and conductivity of electrode material

$$g_i = \frac{h}{\sigma_{\text{bulk}}(1 - \varepsilon_i)S},$$

where σ_{bulk} is the conductivity of bulk electrode: 500 S/cm for lead dioxide and 4800 S/cm for lead.

2.6.4. Component resistances

The applied current is a sum of primary reaction current and gassing currents

$$i_{\text{app}} = i_{\text{app}}^{\text{M}} + i_{\text{app}}^{\text{O}_2} + i_{\text{app}}^{\text{H}_2},$$

where i_{app} is the applied current (A), $i_{\text{app}}^{\text{M}}$ the primary reaction current, $i_{\text{app}}^{\text{O}_2}$ the oxygen reaction current, and $i_{\text{app}}^{\text{H}_2}$ is the hydrogen reaction current.

The charge-transfer resistance (23) combines these component resistances of primary and gassing reactions. It is the resistance of primary reaction if the battery is deep discharged

$$R_{\text{M}} = \frac{\eta}{i_{\text{app}}^{\text{M}}},$$

and it is the overall resistance of oxygen and hydrogen reactions for battery under overcharge, respectively

$$R_{\text{O}_2} = \frac{\eta_{\text{O}_2}}{i_{\text{app}}^{\text{O}_2}}, \qquad R_{\text{H}_2} = \frac{\eta_{\text{H}_2}}{i_{\text{app}}^{\text{H}_2}}.$$

2.6.5. Overall reaction resistance

The overall reaction resistance is a sum of component resistances connected in parallel

$$\frac{1}{R} = \frac{1}{R_{\text{M}}} + \frac{1}{R_{\text{O}_2}} + \frac{1}{R_{\text{H}_2}}.$$

The cell resistance (25) can be calculated by layers (26) for total reaction in three reaction components where local resistances for oxygen and hydrogen reactions are

$$r_i^{\text{O}_2} = \frac{\eta_i^{\text{O}_2}}{A_i^{\text{O}_2} j_i^{\text{O}_2} hS}, \qquad r_i^{\text{H}_2} = \frac{\eta_i^{\text{H}_2}}{A_i^{\text{H}_2} j_i^{\text{H}_2} hS}. \tag{29}$$

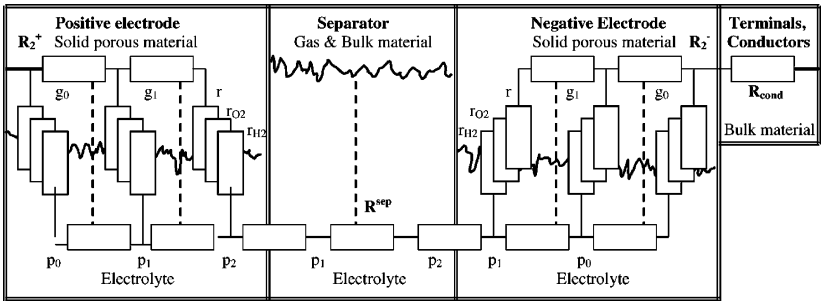

Fig. 1. Distribution of the resistances in electrochemical cell.

The local charge-transfer resistance in (26) should be replaced with component reaction resistances

$$\frac{1}{r_i} = \frac{1}{r_i^{\mathrm{M}}} + \frac{1}{r_i^{\mathrm{O_2}}} + \frac{1}{R_i^{\mathrm{H_2}}}. \tag{30}$$

in order to get the overall reaction resistance.

2.6.6. Conducting elements

The resistance of conducting elements includes

1. grid resistance (bulk electrode);
2. inter-cell connector resistance;
3. connector resistance of battery terminals.

Total resistance of conducting elements is considered as a constant R_{cond}.

2.6.7. Battery resistance

The battery ohmic resistance R_{bat} is a sum of cell resistances and conducting elements resistances

$$R_{\mathrm{bat}} = R_{\mathrm{cell}} + R_{\mathrm{cond}}.$$

2.6.8. Float voltage and polarisation

The float voltage of cell is defined as a sum of equilibrium potential and polarisation $u = U + w$. The polarization is a sum of overvoltage and voltage drop

$$w = \eta + v.$$

Here u is the float voltage, U the equilibrium potential, w the polarization, v is the ohmic voltage drop due to current.

2.6.9. Voltage drop

The ohmic voltage drop depends on current pathways as follows:

$$v = S\sum_{k=0}^{n} i_k^{+}\left(\sum_{j=k}^{n} p_j^{+} + \sum_{j=0}^{k} g_j^{+}\right) + i_{\mathrm{app}}\sum_{j=0}^{n} p_j^{\mathrm{sep}} + S\sum_{k=0}^{n} i_k^{-}\left(\sum_{j=k}^{n} p_j^{-} + \sum_{j}^{k} g_j^{-}\right) + i_{\mathrm{app}} R_{\mathrm{cond}},$$

where i_k is the current density of positive/negative electrode through single layer at depth $x = x_k$, p_j the acid resistance at depth x_j, g_j the electrode resistance at depth x_j and S is the plate area.

The electrode resistance is much lower than acid resistance—500 times lower for positive electrode and 5000 times lower for negative electrode—so it can be ignored.

The voltage drop relationship is simple for the lumped parameter model

$$v = i_{\mathrm{app}}(R_{\mathrm{acid}} + R_{\mathrm{cond}}), \quad R_{\mathrm{acid}} = p^{+} + p_{\mathrm{sep}} + p^{-}.$$

A single current pathway is considered in this case.

2.6.10. Applied model

The battery ohmic resistance is evaluated as a sum of cell resistances and conducting elements resistances in experimental data analysis in Section 3. The conducting elements resistance is considered as a constant. The total cell resistance is calculated using (25), where the component resistances of electrodes and electrolyte calculated using (26) and (27) and using local charge-transfer resistances (24), (29) and (30) and by means of the electrolyte resistance (28).

2.7. Gassing and water loss

Battery gassing is a result of incomplete recombination of oxygen and/or hydrogen evolution. Water dry-out is a consequence of extensive gassing.

2.7.1. Oxygen evaluation and reduction

The oxygen evaluation rate is proportional to the oxygen reaction current on positive electrode

$$\frac{\mathrm{d}\, n_{\mathrm{O_2}}^{\mathrm{evl}}}{\mathrm{d}t} = K_3^{+} i_{\mathrm{app}}^{\mathrm{O_2}^{+}}$$

and the reduction rate is proportional to the oxygen reaction current on negative electrode

$$\frac{\mathrm{d}\, n_{\mathrm{O_2}}^{\mathrm{rec}}}{\mathrm{d}t} = K_3^{-} i_{\mathrm{app}}^{\mathrm{O_2}^{-}},$$

where $n_{\mathrm{O_2}}$ is the number of moles of oxygen generated or reduced on a single electrode (mol) and $i_{\mathrm{app}}^{\mathrm{O_2}}$ is the oxygen reaction current (A).

The reduction rate is proportional to the evolution rate according to steady-state recombination model

$$\frac{\mathrm{d}\, n_{\mathrm{O_2}}^{\mathrm{rec}}}{\mathrm{d}t} = k_{\mathrm{ore}} \frac{\mathrm{d}\, n_{\mathrm{O_2}}^{\mathrm{evl}}}{\mathrm{d}t} \quad \text{or} \quad i_{\mathrm{app}}^{\mathrm{O_2}^{-}} = -k_{\mathrm{ore}} i_{\mathrm{app}}^{\mathrm{O_2}^{+}},$$

where k_{ore} is the oxygen recombination efficiency.

2.7.2. Hydrogen evaluation

The hydrogen evaluation is proportional to the hydrogen reaction current on negative electrode

$$\frac{\mathrm{d}\, n_{\mathrm{H_2}}^{\mathrm{evl}}}{\mathrm{d}t} = K_3^{-} i_{\mathrm{app}}^{\mathrm{H_2}^{-}},$$

where $n_{\mathrm{H_2}}$ is the number of moles of hydrogen (mol) and $i_{\mathrm{app}}^{\mathrm{H_2}^{-}}$ is the hydrogen reaction current on negative electrode.

The hydrogen recombination process on positive electrode is very slow and can be ignored. The hydrogen evaluation current on negative electrode can exceed the corrosion current on positive electrode [3] by value of hydrogen escape current.

The evolution and recombination processes between electrodes are irreversible by switching from discharge to recharge. The potentials for primary reactions are shifted far from the equilibrium potentials for oxygen or hydrogen reactions. This makes reversion impossible. The gassing process during recharge is similar to discharge but more extensive because of more far shift of potentials.

A possible imbalance between evolution and recombination rates will trigger the accumulation process of gasses in free space of battery. The oxygen accumulation and recombination

processes are well balanced in VRLA battery. The hydrogen evolution is progressive accumulation process but is much less extensive than evolution of oxygen

$$\frac{\mathrm{d}n^{\mathrm{g}}_{\mathrm{O_2}}}{\mathrm{d}t} = K_3^{+} i_{\mathrm{app}}^{\mathrm{O_2}^{+}} + K_3^{-} i_{\mathrm{app}}^{\mathrm{O_2}^{-}}, \qquad \frac{\mathrm{d}n^{\mathrm{g}}_{\mathrm{H_2}}}{\mathrm{d}t} = K_3^{-} i_{\mathrm{app}}^{\mathrm{H_2}^{-}},$$

where $n^{\mathrm{g}}_{\mathrm{O_2}}$, $n^{\mathrm{g}}_{\mathrm{H_2}}$ is the number of gas moles (oxygen or hydrogen) accumulated in the free space of battery (mol).

Steady-state process: The following simplified models can be used for approximation of steady-state gassing processes

$$\frac{\mathrm{d}n^{\mathrm{g}}_{\mathrm{O_2}}}{\mathrm{d}t} = \frac{\mathrm{d}n^{\mathrm{evl}}_{\mathrm{O_2}}}{\mathrm{d}t} - \frac{\mathrm{d}n^{\mathrm{rec}}_{\mathrm{O_2}}}{\mathrm{d}t} = (1 - k_{\mathrm{ore}}) \frac{\mathrm{d}n^{\mathrm{evl}}_{\mathrm{O_2}}}{\mathrm{d}t}$$

and

$$2\frac{\mathrm{d}n^{\mathrm{g}}_{\mathrm{H_2}}}{\mathrm{d}t} = \frac{\mathrm{d}n^{\mathrm{g}}_{\mathrm{O_2}}}{\mathrm{d}t}.$$

The hydrogen evolution current is only 1/100 of the oxygen evolution current because of the relationship $2i_{\mathrm{app}}^{\mathrm{H_2}^{-}} = (1 - k_{\mathrm{ore}}) i_{\mathrm{app}}^{\mathrm{O_2}^{+}}$.

The partial pressure of gases is proportional to the number of gas moles in the free space of battery accumulated under closed valve. Pressure that is any higher than the preset opening pressure of valve will trigger gas escape with rates

$$\frac{\mathrm{d}n^{\mathrm{esc}}_{\mathrm{O_2}}}{\mathrm{d}t} = \frac{n^{\mathrm{g}}_{\mathrm{O_2}}}{n^{\mathrm{g}}_{\mathrm{O_2}} + n^{\mathrm{g}}_{\mathrm{H_2}}} (K_3^{+} i_{\mathrm{app}}^{\mathrm{O_2}^{+}} + K_3^{-} i_{\mathrm{app}}^{\mathrm{O_2}^{-}}),$$

$$\frac{\mathrm{d}n^{\mathrm{esc}}_{\mathrm{H_2}}}{\mathrm{d}t} = \frac{n^{\mathrm{g}}_{\mathrm{H_2}}}{n^{\mathrm{g}}_{\mathrm{O_2}} + n^{\mathrm{g}}_{\mathrm{H_2}}} K_3^{-} i_{\mathrm{app}}^{\mathrm{H_2}^{-}}.$$

The water dry-out equals to hydrogen escape through valve

$$\frac{\mathrm{d}n_{\mathrm{H_2O}}}{\mathrm{d}t} = \frac{\mathrm{d}n^{\mathrm{esc}}_{\mathrm{H_2}}}{\mathrm{d}t}.$$

Here $n_{\mathrm{H_2O}}$ is the number of water moles of dry-out (mol).

High water loss (over 10%) can drastically affect battery performance. Batteries with more than 15–20% water loss are replaced in most applications [11].

3. Experiment

The proposed model was tested experimentally. It was first calibrated and then its accuracy was evaluated against the measured data. A simple testing system, shown in Fig. 2, was used to record measured data in the experiment.

3.1. Experiment

Four batteries, connected in a string and placed into a container, were charged and discharged periodically at elevated temperature of 40–50 °C. The batteries were charged up to 99–100% of real capacity and discharged to under 5–10%. A relatively low charging voltage of 2.22 VPC was used to prevent increased water decomposition during extended charging of 25 h. The applied current and float voltage of batteries, as well as temperature in the container, were measured and recorded continuously.

The data presented in this paper is relevant to the following operation of batteries. A string of fully charged batteries was discharged after 1 day of rest with constant current at rate $C_{10}/I = 5.6$ h and then charged at rate $C_{10}/I = 4.6$ h for a short period until the voltage of 2.20 VPC was reached. The charging current was reduced further gradually to maintain approximately constant voltage at 2.22 VPC (i.e. average value over all cells of batteries in string). Actually, increasing voltage from 2.20 to 2.24 VPC was carried out in the experiment. This made sure that all batteries were charged completely like they are charged in the taper charging procedure.

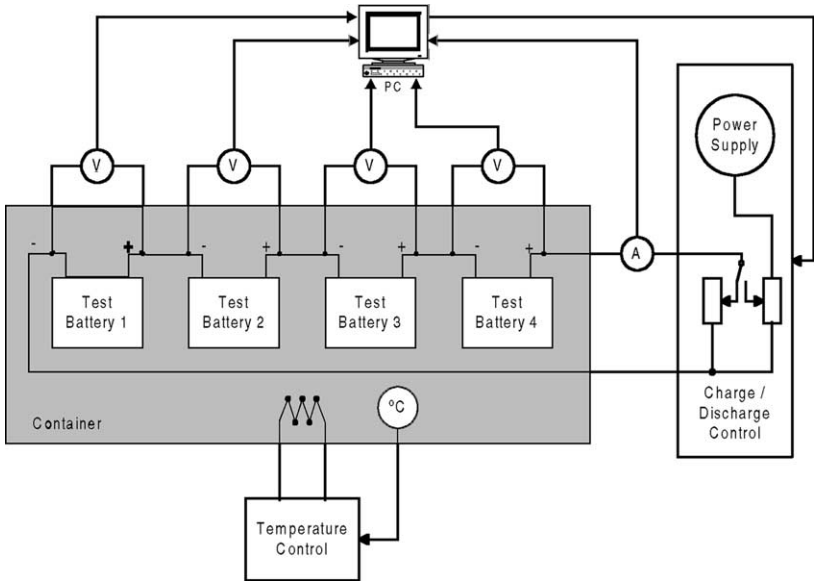

Fig. 2. Battery testing system.

Two sets of batteries A and B from the same manufacturer were used for testing.

Specification: type: VRLA battery, GEL technology; nominal voltage: 12 V; capacity: $C_{10} = 28$ Ah or more; cut-off time: 5, 10 or 20 h at discharge current of 5.1, 2.8 or 1.6 A for cut-off voltage 1.70–1.75 VPC.

Battery design: number of sections: 6; number of positive plates: 4; negative plates: 3; plate height: 11.3; width: 15.4 cm; thickness of positive plate: 0.23, negative plate: 0.22 cm; thickness of separator: 0.36 cm.

A lumped parameter model is used for data analysis in this paper. It has the same approximation accuracy as the distributed parameter model. The charge–discharge rates of the experiment are relatively low (4–6 h). The electrochemical processes are in weak dependence on the location in electrode [19] for rates that are over 1–2 h. The lumped parameter model used was obtained as a modification of the distributed parameter model approximated with a single layer per electrode.

3.2. Model calibration

The model calibrated earlier [19] on the same type of batteries is partially used in this paper. Adaptation is made with respect to a new string. A different string of batteries was used in the earlier paper. There it was detected that battery 2 is the weakest link of the string. Its calibrated model is applied on batteries 2 and 3 in this paper. They were tested here as the weakest link of the string. The SOC-related tortuosity exponent (3) for discharge process (i.e. electrode morphology) was changed between these batteries (Table 1).

The new calibration data for electrodes and separator thickness is presented in Table 2.

The primary reaction was analysed in the earlier paper without gas formation processes. However, some minor gassing took place in the experiment. This gassing was formally contributed into the parameters of (2). The gassing process is accounted for separately in this paper. New calibrated values of parameters of (2) are shown in Table 3.

Table 1
Electrode morphology

Battery number	Positive electrode	Negative electrode
B1, B4	0.45	0.39
B2, B3	0.26	0.22

Table 2
Thickness of electrodes and separator

Battery number	Positive electrode	Separator (mm)	Negative electrode
B1	0.490	2.334	0.381
B2	0.474	2.277	0.363
B3	0.473	2.269	0.364
B4	0.490	2.351	0.382

Table 3
Charging exponent

Battery number	Positive electrode, ρ	Negative electrode, ρ	Both electrodes, γ
B1	11.09	11.16	5.642
B2	8.987	8.393	5.271
B3	9.369	8.680	5.295
B4	13.13	10.93	5.466

Table 4
Charging efficiency

Parameter	B1	B2	B3	B4
α_{Ah}	0.921	0.931	0.933	0.918

The charging efficiency factor is important for extended charging its calibrated values are presented in Table 4.

No other changes were made in the calibrated model with respect to the primary reaction.

The gassing process model is calibrated in this paper using similar identification method as earlier. The calibration results are shown for oxygen reaction in Table 5. They are shown in the same minimal collection as they were applied for data analysis.

The following data was used as constants in the calculation algorithm:

1. oxygen flow velocity through separator: $Q = 3.6$ mm/h;
2. oxygen recombination efficiency: $k_{ore} = 0.99$;
3. equilibrium potentials versus hydrogen electrode: $U_{O_2} = 1.23$ V for oxygen, $U_{H_2} = 0$ V for hydrogen.

3.3. Model accuracy

The charge–discharge behaviour of the batteries under test was predicted as follows.

The applied current for the model was chosen as close as possible to the one measured in the experiment. A special control algorithm was used to stabilise the applied current of the model at measured values. The feedback control drives overpotential on both electrodes and, eventually, the electrochemical reaction to make the tracking errors minimal. High tracking accuracy was obtained (Fig. 3). The model current can emulate the measured current in many details including the perfect charging curve and deviation of the measured current from the perfect curve. The tracing error is relatively large during transition from discharge to recharge for a short period (10–20 min). It can be reduced somewhat

Table 5
Oxygen reaction parameters

Parameter	B1	B2	B3	B4
i_{0,O_2} (pA/m^2)	2.650	1.490	1.940	5.900
α_{a,O_2}	0.670	0.701	0.693	0.635

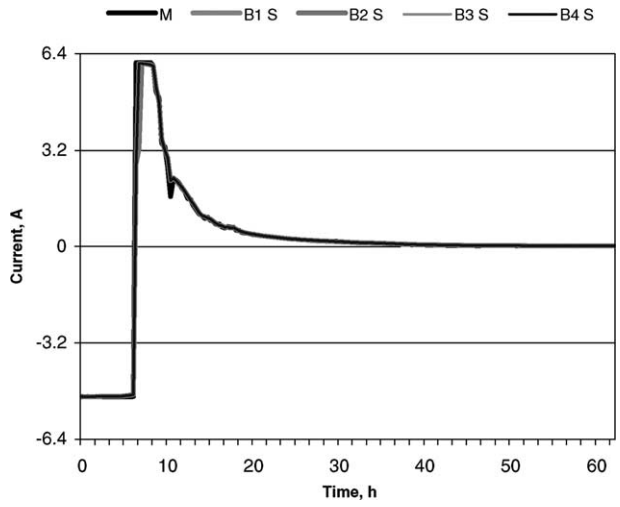

Fig. 3. Applied current profile. The measured current (M) and model reproduced currents (S) are almost identical except for some differences during the transaction from discharge to recharge.

smaller using shorter sampling interval. Relatively large sampling interval (20 s) was used to facilitate fast calculation. The calculation speed of one physical second per one hour of battery time was achieved with this sampling interval (on a 533 MHz Pentium III PC).

3.3.1. Model accuracy

Typical charging curves are shown in Fig. 4. They were first measured and later predicted using the model. The prediction accuracy is high. The model can predict measured voltage in full range of charge–discharge processes including deep discharge and overcharge. The following situation is demonstrated in Figs. 4 and 5. Higher voltage is measured

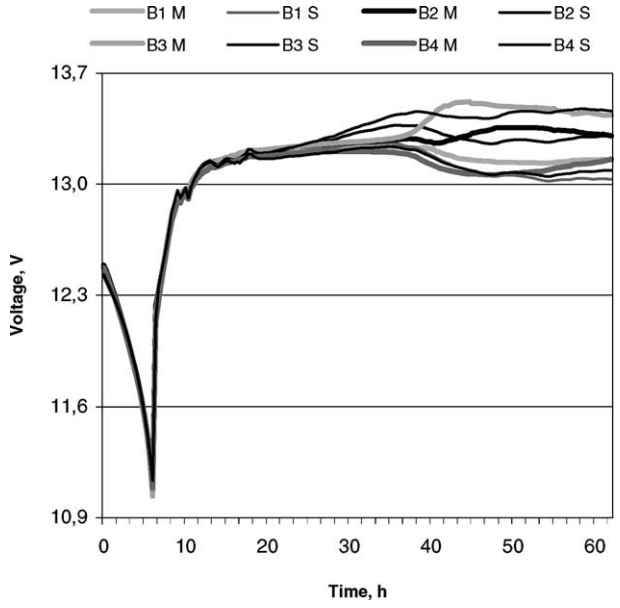

Fig. 4. Typical charging curves of tested batteries. Model-predicted and measured voltage is shown as a pair of fine and bold lines in the closest neighbourhood for every battery.

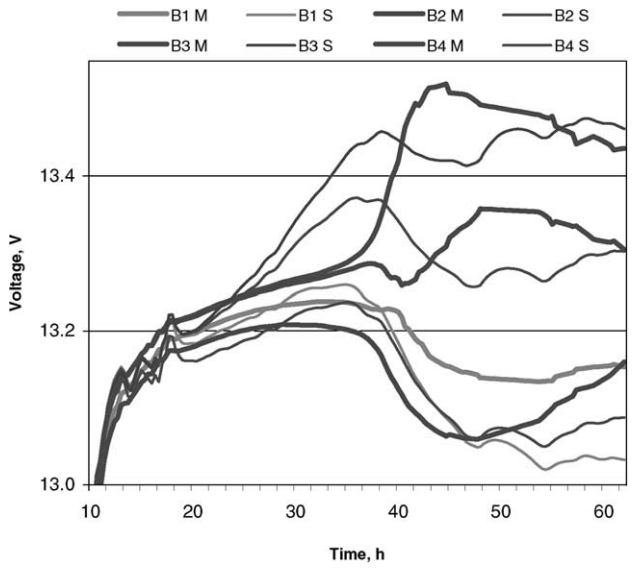

Fig. 5. This figure is a zoom of Fig. 4 for overcharge, showing charge–discharge voltage on tested batteries: model-predicted (S) and measured (M) voltage. The model can predict measured voltage in full range including overcharge.

on batteries 2, 3 and lower voltage on batteries 1, 2 during overcharge (the string voltage is constant). Respectively, higher voltage is model-predicted on batteries 2, 3 and lower voltage on batteries 1, 2.

The two-step reaction model for negative electrode (8) suggested in [16] was tested against single-step reaction model (4). The limit current density $I_{PbSO_4} = 1$ A/cm^2 in two-step reaction model was chosen from best fit with experimental data. However, the prediction accuracy for single- and two-step reaction models was similar for all the tested batteries. Therefore, simpler single-step reaction model was used for further analysis.

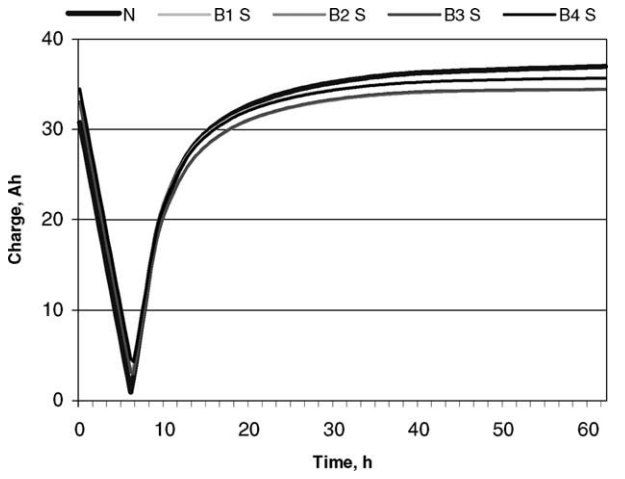

Fig. 6. State-of-charge: model-predicted charge (S) and charge calculated by applied current (N). The capacity of batteries (calculated by applied current) is overestimated while model-predicted capacity is more realistic.

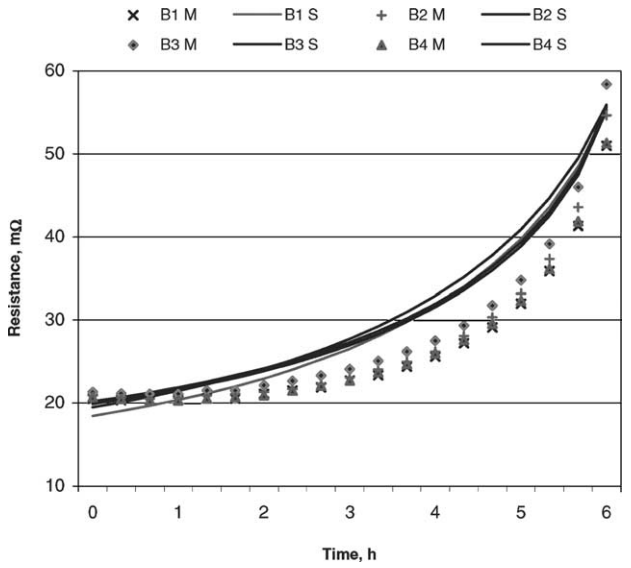

Fig. 7. Ohmic resistance: model-predicted resistance (S) and resistance measured by direct current method (M) during discharge.

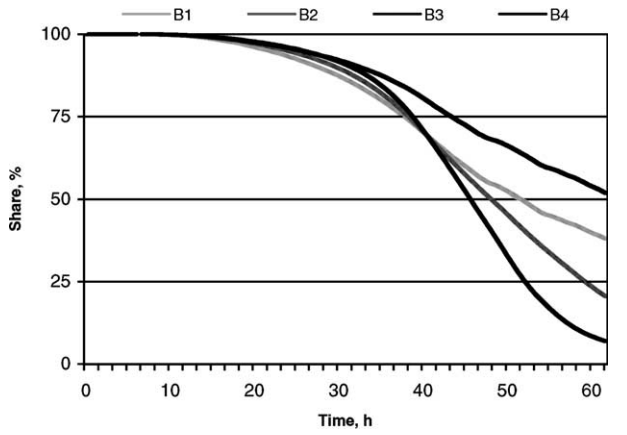

Fig. 8. Share of applied current between primary and gassing reactions evaluated using the model and the current, voltage and temperature measurements. The charging turns quickly into extensive gassing for the batteries 2, 3.

3.3.2. State-of-charge

The state-of-charge is shown in Fig. 6 for full cycle of charge–discharge processes; the model-predicted charge and the charge calculated by applied current are shown. The model predicted capacity (maximum charge) of 36, 34, 34 and 36 Ah is lower than the capacity of 37 Ah computed using applied current. This is because the applied current is higher than real charging current due to heat generation and dissipation, current loss through isolation and water decomposition in battery.

3.3.3. Resistance

The battery ohmic resistances measured with direct-current method during discharge are shown in Fig. 7. The measured resistance is compared with model-predicted values. Here, as an exception, a distributed parameter model with six layers per each electrode was used. The distributed parameter model can approximate the charge-transfer resistance and conductivity in electrodes more accurately than the lumped parameter model. However, the prediction accuracy is not very high. The model predicts smoother changes of resistance than measured.

The measured resistance is a good indicator of battery capacity in deep discharge. Unfortunately, these measurements are not applicable for testing of fully-charged batteries.

4. State estimation

The calibrated model can be applied for the evaluation of the unobservable processes in battery using observable processes. The gas formation processes are evaluated and analysed using current–voltage and temperature measurements in this section. Their possible use in battery monitoring is discussed.

A retrospective analysis is applied. The unobservable processes are evaluated by means of theoretical cell model, using current–voltage and temperature measurements recorded experimentally in charge–discharge processes. The cell model calibrated previously in another experiment for the same batteries is used for analysis beside measured current, voltage and temperature processes.

Charging efficiency: The share of applied current between primary and gassing reactions is in favour of gassing reaction during overcharge (Fig. 8). The charging process is ineffective during overcharge—it is up to 15 times slower than gassing reaction by share of current that depends on battery. The primary reaction current is lower for batteries 3 and 2 than for batteries 1 and 2.

4.1. Gas formation

The terms ‘‘initial-charge period’’, ‘‘float-charge period’’, ‘‘overcharge period’’ and ‘‘voltage disburse’’ are used as follows.

The initial charging period when constant current is applied is the initial-charge period.

The limited charging period between initial-charge and overcharge periods is the float-charge period. A constant voltage is applied to limit current in this period.

The inflation or deflation of voltages of single batteries during overcharge is the voltage disburse.

The charging period after the disburse of voltages starts is the overcharge period. Exact timing of disburse can be observed from charging curves (Fig. 4).

4.1.1. Oxygen current

All batteries in a string were charged rather completely to reach the state of overcharge. Battery 1 was charged up to 99.4% of maximum capacity, battery 2 to 99.9%, battery 3 to

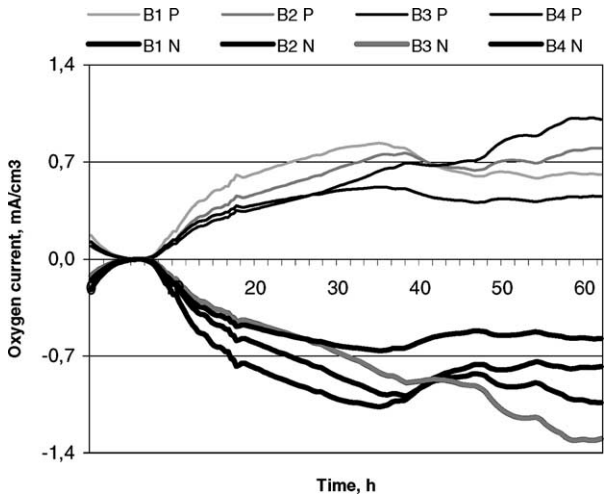

Fig. 9. Oxygen evolution and recombination current on positive (P) and negative (N) electrodes evaluated using the model and the current, voltage and temperature measurements. These oxygen evolution and recombination processes are well balanced.

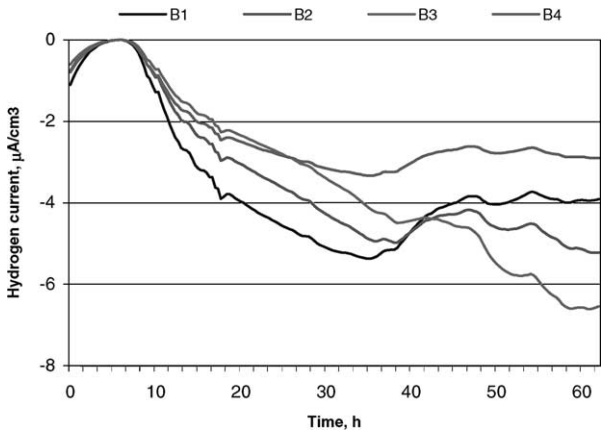

Fig. 10. Hydrogen evolution current on negative electrodes evaluated using the model and the current, voltage and temperature measurements. This current is much smaller than oxygen evolution current.

99.9%, battery 4 to 99.4%. The voltage disburse starts at 98% of maximum capacity for all batteries. The applied current was nearly equal to the primary reaction current until this point (98%) was reached, from there further on the primary reaction current was increasingly more and more compensated by oxygen evolution and recombination current (Fig. 8) and a little by hydrogen evolution current (Fig. 9). These secondary processes are less stable; they depend on gas formation and transport through separator.

Symmetry between the evolution and recombination processes is good for oxygen (Fig. 9). The recombination efficiency is either nearly constant or a time-varying process in a very narrow band.

4.1.2. Float-charge period

The oxygen evolution and recombination currents are slightly higher for batteries 1 and 4 than for batteries 2 and 3 during float-charge period. This difference cannot be observed directly from measured data, it is masked by high current of the main reaction.

4.1.3. Overcharge period

The oxygen current for battery 3 is higher than for other batteries during overcharge; for battery 2 it has an increasing trend. Difference between the batteries is observable by oxygen current during overcharge (Fig. 9), it is large enough not to be masked by the current of main reaction. The oxygen current can be used to distinguish between seemingly equal batteries under overcharging.

4.1.4. Hydrogen current

The hydrogen evolution current is slightly higher for batteries 1 and 4 than for batteries 2 and 3 during the float-charge period (Fig. 10). This difference cannot be observed directly from measured data, but is masked by high current of primary reaction or oxygen reaction. The hydrogen current for battery 3 is higher than for other batteries during overcharge. The hydrogen current cannot be used to distinguish between seemingly equal batteries.

4.1.5. Gas escape and water loss

The gas escape and water dry-out evaluated using the observable current–voltage measurements are shown in Figs. 11 and 12.

Initial-charge period: The gas escape is small during the initial-charge period but it increases substantially during the float-charge period and before or during the overcharge period depending on battery. A high primary reaction current can be produced with relatively low overvoltage during initial-charge period. This overvoltage is not sufficient to produce current of the secondary reactions, they are hindered by the low value of state-of-charge.

Float-charge period: When the charging proceeds at constant voltage, it will be more difficult to produce the

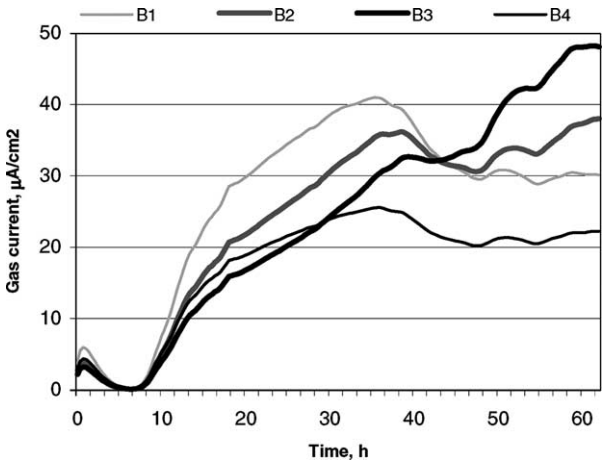

Fig. 11. Gas reaction current of tested batteries evaluated using the model and the current, voltage and temperature measurements. This is mainly oxygen reaction current.

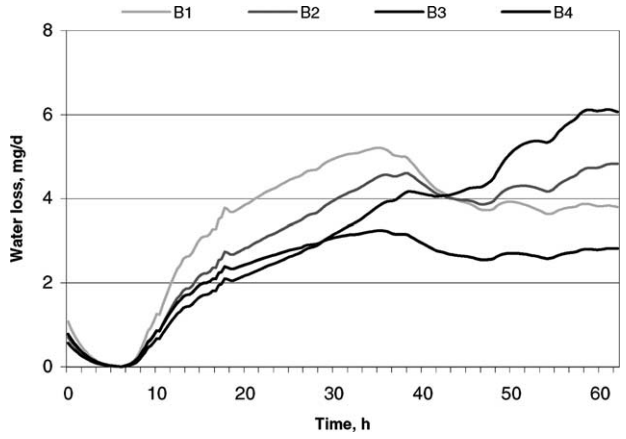

Fig. 12. Water drying out evaluated using the model and the current, voltage and temperature measurements. It is in good correlation with oxygen reaction current in Fig. 11.

current of primary reaction because of reaction hindrance with increased value of state-of-charge. As a result, higher overvoltage should be applied. This produces more current in secondary reactions than in primary reaction. Both oxygen and hydrogen currents are relatively high during the float-charge period (Figs. 9 and 10).

Overcharge period: In the next period there will be a drop of gassing current because of lower current demand. It is mainly compensated by oxygen current. The oxygen evolution is a more productive process than hydrogen evolution, especially for high value of state-of-charge. The oxygen evolution current is high but still in good balance with recombination current. As a result, it has little effect on oxygen escape. The primary reaction is completely hindered during overcharge. The water loss at the end of charging processes is relatively small. Ageing of batteries 1 and 4 is less during the overcharge than it was during the main charge period.

The disburse of voltage is not related to electrolyte density or conductivity during overcharge, there are no changes as shown in Fig. 13.

4.2. On relation of capacity and overcharge voltage

The solution of the battery monitoring problem could be simplified if some simple indicators of the state-of-health of battery would be found. Unfortunately, it seemed unlikely. The float voltage during overcharge or resistance cannot be used as simple indicators. This is shown on the basis of measured and evaluated data in the following example.

Example 1. Higher voltage during overcharge may predict lower capacity. For example, the voltage of batteries 2 and 3 is higher and the capacity lower in comparison with batteries 1 and 2. This conclusion can be made comparing the predicted voltage for overcharge and the state-of-charge in Figs. 4 and 6. The same conclusion can be made by inspection of the measured voltage in dependence of the degree of discharge or recharge in Figs. 14 and 15. Lower cut-off voltage will turn into the higher voltage during overcharge.

Unfortunately, this is not true in general. Higher voltage during overcharge may predict lower capacity. This is shown in Fig. 16 for another set of batteries during deep discharge and overcharge periods.

High charge-transfer resistance during overcharge can explains high float voltage for both sets of batteries. This is shown in Fig. 17 (for basic set). The ohmic resistance in batteries 2 and 3 is higher than in batteries 1 and 2.

Battery resistance and capacity are related through charge-transfer resistance for primary reaction. This relationship is well observable in the condition of deep dis-

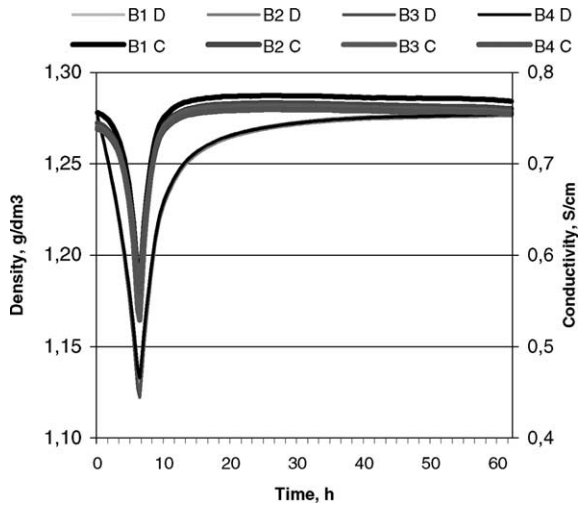

Fig. 13. Electrolyte density (*D*) and conductivity (*C*) evaluated using the model and the current, voltage and temperature measurements. The voltages disburse in Fig. 4 is not affected by electrolyte concentration or conductivity.

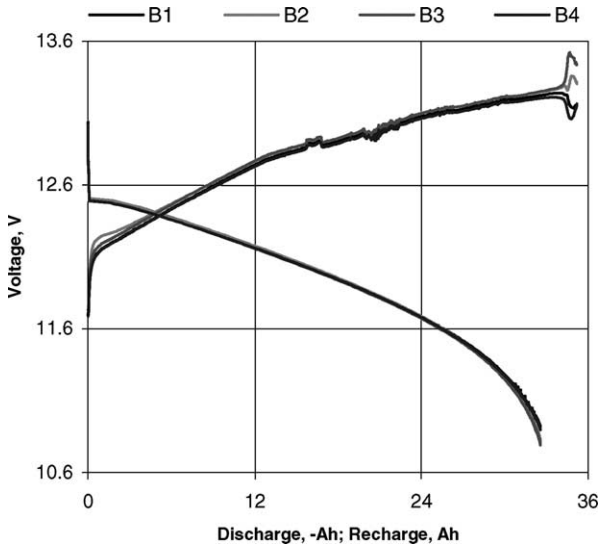

Fig. 14. Measured voltage of batteries shown in dependence on the degree of discharge or recharge.

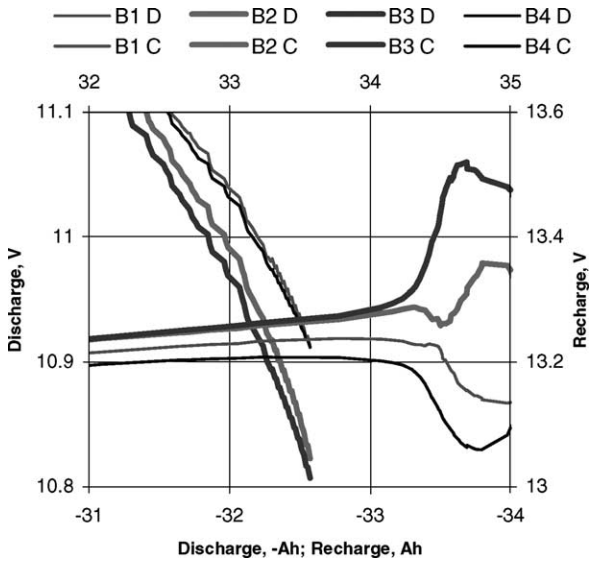

Fig. 15. This figure is a zoom of Fig. 14 for deep discharge (D) and overcharge (C). The lower cut-off voltage will turn into the higher voltage during overcharge.

charge. Unfortunately, it is not observable on well-charged battery due to the lack of primary reaction. The charge-transfer resistance of primary reaction is masked by large values of the charge-transfer resistance of gassing reactions. The battery ohmic resistance and battery capacity are not related during overcharge.

Therefore, float voltage during overcharge cannot be used as an indicator of battery capacity nor resistance.

No evidence that the state-of-health of a battery can be detected with some simple indicator like resistance or float

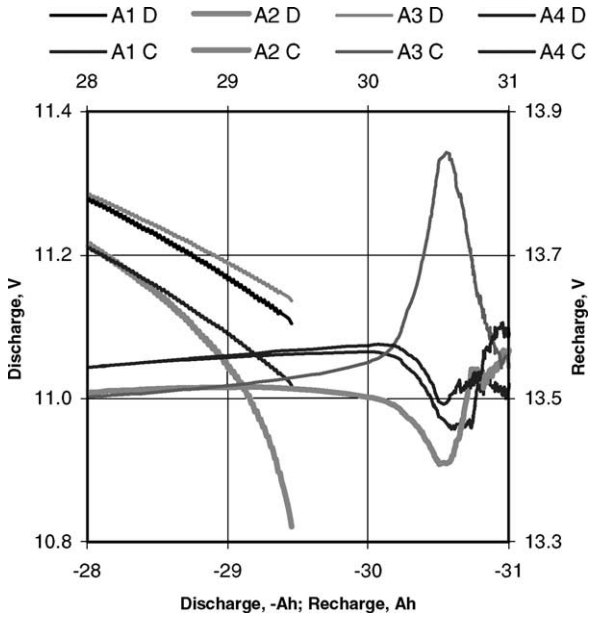

Fig. 16. Measured voltage of another set of batteries shown for deep discharge and overcharge The lower cut-off voltage will turn into lower voltage during overcharge for this set of batteries.

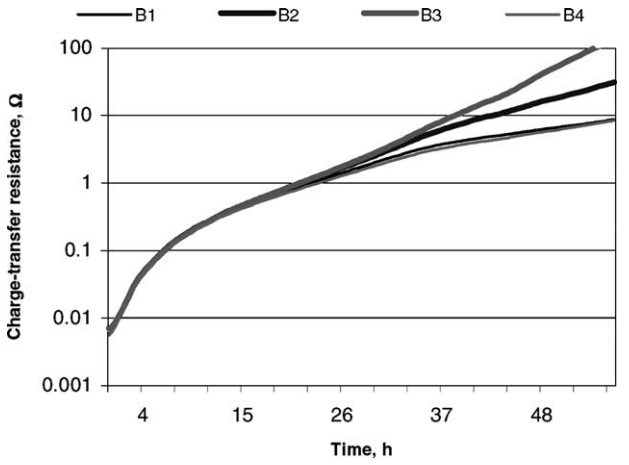

Fig. 17. Charge-transfer resistance evaluated using the model and the current, voltage and temperature measurements. High resistance predicts high float voltage during overcharge.

voltage during overcharge. The state-of-health can be detected using a complex model-based method. It can be evaluated in the form of natural electrochemical processes by direct current–voltage and temperature measurements from model.

5. Conclusion

A theoretical model based on the internal electrochemical processes of VRLA battery was introduced that may be used to predict the unobservable processes such as reaction rate, overpotential, current density, porosity, acid concentration, gassing, water dry-out and other electrode parameters by observable current–voltage and temperature measurements. The introduced model was a modified version of the previously presented model [19] with respect to gassing and other processes. It was calibrated on measured data and tested against experiment. High prediction accuracy was demonstrated relevant to the full discharge–recharge cycle including deep discharge and overcharge of a battery. The case sensitive prediction of individual behaviour of batteries during overcharge was shown possible.

References

[1] D.M. Bernardi, M.K. Carpenter, A mathematical model of the oxygen-recombination lead-acid cell, J. Electrochem. Soc. 142 (8) (1995) 2631–2642.
[2] D.M. Bernardi, H. Gu, A.Y. Schoene, Two-dimensional mathematical model of a lead-acid cell, J. Electrochem. Soc. 140 (8) (1993) 2250–2258.
[3] D. Berndt, Maintenance-Free Batteries, Research Studies Press/Wiley, New York, 1997, 496 pp.
[4] D. Berndt, R Bräutigam, U. Teutsch, Temperature compensation of float voltage, in: Proceedings of the Seventh International Telecommunications Energy Conference on The Special Situation of VRLA Batteries, The Netherlands, 1995, pp. 1–12.

[5] E.C. Dimpault-Darcy, T.V. Nguyen, R.E. White, A two-dimensional mathematical model of a porous lead dioxide electrode in a lead-acid cell, J. Electrochem. Soc. 135 (2) (1988) 278–285.
[6] P. Ekdunge, D. Simonsson, The discharge behaviour of the porous lead electrode in lead-acid battery. I. Experimental investigation, J. Appl. Electrochem. 19 (1989) 127–135.
[7] P. Ekdunge, D. Simonsson, The discharge behaviour of the porous lead electrode in lead-acid battery. II. Mathematical model, J. Appl. Electrochem. 19 (1989) 136–141.
[8] H. Gu, T.V. Nguyen, R.E. White, A mathematical model of a lead-acid cell: discharge, rest and charge, J. Electrochem. Soc. 134 (12) (1987) 2953–2960.
[9] H. Gu, C.Y. Wang, B.Y. Liaw, Numerical modeling of coupled electrochemical and transport processes in lead-acid cell, J. Electrochem. Soc. 144 (6) (1997) 2053–2061.
[10] W.B. Gu, G.O. Wang, C.Y. Wang, Modeling the overcharge process of VRLA batteries, in: Proceedings of the 16th Annual Battery Conference on Application and Advantages, 2001, pp. 181–186.
[11] H. Huang, T.V. Ngyen, A two-dimensional transient thermal model for valve-regulated lead-acid batteries under overcharge, J. Electrochem. Soc. 144 (6) (1997) 2062–2068.
[12] F. Huet, A review of impedance measurements for determination of the state-of-charge or state-of-health of secondary batteries, J. Power Sources 70 (1998) 59–69.
[13] J. Landfors, D. Simonsson, A. Sokirko, Mathematical modelling of a lead-acid cell with immobilized electrolyte, J. Power Sources 55 (1995) 217–230.
[14] B.Y. Liaw, K. Bethune, in: Proceedings of the 16th Annual Battery Conference on Validation of the Modeling of Overcharge Process in VRLA Cells, 2001, pp. 187–192.
[15] J. Newman, W. Tiedemann, Porous-electrode theory with battery applications, chemical engineering research and development, AIChE J. 21 (1) (1975) 25–41.
[16] J. Newman, W. Tiedemann, Simulation of recombination lead-acid batteries, J. Electrochem. Soc. 144 (9) (1997) 3081–3091.
[17] T.V. Nguyen, R.E. White, H. Gu, The effects of separator design on the discharge performance of a starved lead-acid cell, J. Electrochem. Soc. 137 (10) (1990) 2998–3004.
[18] D. Simonsson, P. Ekdunge, M. Lindgren, Kinetics of the porous lead electrode in the lead-acid cell, J. Electrochem. Soc. 135 (7) (1988) 1614–1618.
[19] A. Tenno, R. Tenno, T. Suntio, Charge–discharge behaviour of VRLA batteries: model calibration and application in state estimation and failure detection, J. Power Sources 103 (2001) 42–53.
[20] W.H. Tiedemann, J. Newman, in: S. Gross (Ed.), Battery Design and Optimization, The Electrochemical Society Softbound Proceeding Series, Princeton University Press, New York, 1979, 23 pp.